The functional specificity of ERECTA-family receptors in *Arabidopsis* stomatal development is ensured by molecular chaperones in the endoplasmic reticulum

Ke-Zhen Yang[1,7], Chao-Ran Zuo[1,2,7], Ya-Jun Leng[3,‡], Jun-Ling Yue[1,2], Hui-Chao Liu[1,2], Zhi-Bin Fan[1,2], Xue-Yi Xue[4], Juan Dong[5,6], Li-Qun Chen[3,*] and Jie Le[1,2,*]

[1]Key Laboratory of Plant Molecular Physiology, CAS Center for Excellence in Molecular Plant Sciences, Institute of Botany, Chinese Academy of Sciences, Beijing 100093, China

[2]University of Chinese Academy of Sciences, Beijing 100049, China

[3]State Key Laboratory of Plant Physiology and Biochemistry, College of Biological Sciences, China Agricultural University, Beijing 100193, China

[4]Department of Plant Biology, University of Illinois at Urbana-Champaign, Urbana, IL 61801, USA

[5]Waksman Institute of Microbiology, Rutgers, The State University of New Jersey, Piscataway, NJ 08854, USA

[6]Department of Plant Biology, Rutgers, The State University of New Jersey, New Brunswick, NJ 08901, USA

*Correspondence: chenliqun@cau.edu.cn and lejie@ibcas.ac.cn

[‡]These authors contributed equally to this article

KEY WORDS: *Arabidopsis*, Stomatal development, ERECTA receptor, SDF2-ERdj3B-BiP, Molecular chaperone, ERQC.

SUMMARY: The redundant but distinct roles of ERECTA-family receptors in stomatal development are ensured by the molecular chaperone complexes that preferentially maintain protein abundance and proper subcellular dynamics.

ABSTRACT

Stomata are epidermal pores that control gas exchange between plants and the atmosphere. In *Arabidopsis*, the ERECTA family (ERECTAf), including ERECTA, ERECTA-LIKE1 (ERL1), and ERL2, redundantly play pivotal roles in enforcing the so-called “one-cell-spacing” rule. Accumulating evidences demonstrated that the functional specificities of receptors are likely associated with their differential subcellular dynamics. The endoplasmic reticulum (ER)-resident chaperone complex SDF2-ERdj3B-BiP functions in many aspects of plant development. We employed pharmacological treatments combined with cell biological and biochemical approaches to demonstrate that the abundance of ERECTA was reduced in *erdj3b-1* mutant, but the localization, and dynamics of ERECTA were barely affected. By contrast, the *erdj3b* mutation caused the retention of ERL1/ERL2 in the ER. Furthermore, we found that the function of SDF2-ERdj3B-BiP is implicated with the distinct roles of ERECTAf receptors. Our findings establish that the ERECTAf receptor-mediated signaling in stomatal development is ensured by the activities of ER quality control system (ERQC) that preferentially maintain protein abundance of ERECTA and proper subcellular dynamics of ERL1/ERL2, respectively, prior to the receptors reaching their destination, the plasma membrane, to execute their functions.

INTRODUCTION

Stomata are epidermal pores that play important roles in gas exchange between plants and the atmosphere. In *Arabidopsis*, a subpopulation of protodermal cells adopts the stomatal lineage identity to become the Meristemoid Mother Cells (MMC). A MMC undergoes asymmetric cell division to create two daughter cells with distinct identity, a smaller Meristemoid (M) and a larger Stomatal Lineage Ground Cell (SLGC). Both Ms and SLGCs have the potential to further divide asymmetrically, but each has different cell-fate trajectory. Ms will differentiate into Guard Mother Cell (GMC) and eventually produce a pair of kidney-shaped Guard Cells (GC) after GMC symmetric division. SLGCs will ultimately become puzzle-shaped pavement cells in the epidermis (Nadeau and Sack, 2002; Dong and Bergmann, 2010; Torii, 2012).

Stomatal formation and pattern comply with the so-called “one-cell-spacing” rule, by which each stoma is spaced out by at least one pavement cell. It was believed that short-distance signaling mediated by peptide ligand-receptor signal transduction specifies cell-to-cell communication during stomatal pattern formation. The identified key components include secretory peptides of the EPIDERMAL PATTERNING FACTOR (EPF)/EPF-LIKE (EPFL) family (Hunt and Gray, 2009; Sugano et al., 2010), the Leucine-Rich Repeat (LRR) receptor protein TOO MANY MOUTHS (TMM) (Nadeau and Sack, 2002), and the ERECTA-family (ERECTAf) and SERK-family receptors (Meng et al., 2015; Shpak et al., 2005). Three ERECTAf receptors, including ERECTA, ERECTA-LIKE1 (ERL1), and ERL2, redundantly govern the initial decision of stomatal lineage in the epidermis. The fine-scale genetic analyses revealed that individual members may contribute differently to stomatal division and differentiation. Loss-of-function of all three ERECTAf genes caused large stomatal clustering. The single mutation of *erecta* resulted in excessive stomatal precursor-like cells that failed to differentiate into mature stomata. With an additional *erl2* mutation in *erecta erl2* double mutants, the formation

of excessive precursor-like cells enhanced. By contrast, additional mutation of *erl1* promoted the differentiation of arrested precursor-like cells into stomata in *erecta* and *erecta erl2* double mutants (Shpak et al., 2005). Thus, although the collective function of the ERECTA family is to suppress stomatal initiation, individual members contribute differently to different aspects in stomatal division and differentiation (Shpak et al., 2005).

In eukaryotic cells, secretory proteins, including cell-surface receptors, are synthesized by the endoplasmic reticulum (ER)-bound ribosomes. Nascent proteins are then translocated into the ER lumen where carbohydrates are added primarily to newly synthesized, unfolded proteins. As the above processes are error-prone, the eukaryotic cells have ER quality control (ERQC) system that monitors protein conformation and eliminates terminally misfolded polypeptides through ER-associated degradation (ERAD) or autophagic degradation (Strasser, 2018).

The maintenance of protein homeostasis of cell-surface receptors involves ERQC events in plants. For example, misfolded growth receptor BRASSINOSTEROID INSENSTITIVE 1 (BRI1) was shown to retain in the ER and degraded by a glycan-dependent ERAD process (Hong et al., 2012). Limited evidences already showed that VAP-RELATED SUPPRESSOR OF TMM (VST) proteins facilitate ERECTAf signal transduction, possibly through a direct interaction between VST and ERL2, and VST can interact with ER-localized protein SOYBEAN GENE REGULATED BY COLD-2 (SRC2) (Ho et al., 2016). Also, it was recently shown that EPFL9/Stomagen triggers the retention of ERL1 in the ER (Qi et al., 2020).

The ER-resident SDF2-ERdj3-BiP chaperone complex plays an important role in protein folding, maturation, and degradation in ERQC (Buchberger et al., 2010; Strasser, 2018). In *Arabidopsis*, *BiPs* have three homologues in the genome (*BiP1*, *BiP2*, and *BiP3*), and no phenotype was found in the single mutant under normal conditions, but the high-order mutants displayed pollen development defect (Yamamoto et al., 2008; Maruyama et al., 2014a;

Maruyama et al., 2014b). There are two *ERdj3* homologues in *Arabidopsis*, including *ERdj3A/TMS1* and *ERdj3B*. *ERdj3A/TMS1* is mainly expressed in pollen, and its mutation in L*er* background led to pollen defect at high temperatures (Yang et al., 2009). By contrast, *ERdj3B* is widely expressed in all organs, but no obvious phenotype was found in the *erdj3b* single mutant. Recent results showed that *ERdj3B* was involved in anther and ovule development at high temperatures (Yamamoto et al., 2020; Leng et al., 2022). However, whether the SDF2-ERdj3B-BiP chaperone complex is required for stomatal development through regulating ERECTAf receptors has not been experimentally examined.

Here, we employed pharmacological treatments combined with genetic, cell biological and biochemical strategies to demonstrate that, among the stomatal receptors, individual ERECTAf receptors are distinctly modulated by the SDF2-ERdj3B-BiP chaperone complex. Despite of high similarity at the amino-acid sequence among the ERECTAf receptors, SDF2-ERdj3B-BiP chaperone complex appears to maintain the protein abundance of ERECTA, whilst specifically promote the ER exit and translocation of ERL1/ERL2 to the plasma membrane (PM).

RESULTS

ER stress influences the action of ERECTAf receptors

Protein N-glycosylation is closely linked with protein folding and plays an important role in ERQC (Helenius and Aebi, 2004). Several conserved N-glycosylation motifs have been predicted in the LRR ectodomain of all three ERECTAf receptors (Chakraborty et al., 2019). To assay possible involvement of ERQC in stomatal development, wild-type *Arabidopsis* seedlings were treated with tunicamycin (TM), an inhibitor of N-glycosylation (Olden et al., 1982). At a low concentration (30 ng/mL), no obvious stomatal phenotype was found (Fig. 1A, B), but a high concentration (60 ng/mL) of TM induced the

formation of stomatal clusters (Fig. 1C), consistent with previous observation (Ho et al., 2016). When higher concentrations of TM (120 ng/mL or 240 ng/mL) were applied, the stomatal clustering phenotype became more severe and unpaired guard cells within stomatal clusters appeared (Fig. 1D-F). Thus, TM treatment affects stomatal development in a dosage dependent manner.

ERECTAf-receptors redundantly regulate the initial decision and distribution of stomatal lineage in epidermis (Shpak et al., 2005). Due to the redundant function of ERECTA in stomatal patterning control, stomatal phenotype in *erl1-5 erl2-3* double mutant is normal (Fig. 1G). However, the TM-induced stomatal clustering phenotype in *erl1-5 erl2-3* is more severe than that found in wild-type cotyledons after 60 ng/mL TM treatment (Fig.1H vs. 1C). For instance, about 37% stomatal units in *erl1-5 erl2-3* consist of more than 4 GCs, compared with 10% in the wild type, indicating a redundant function of ERECTA in resistance to TM-induced stomatal clustering (Fig. 1I).

We analyzed expression level and subcellular localization of the fluorescent protein-tagged ERECTAf receptors. *ERECTA:ERECTA-YFP* complemented the stomatal phenotype of *erecta* mutant (*er-105*) and predominantly localized at the PM in all epidermal cells (Fig. 1J). After TM treatment for 24 hours, no obvious differences in the expression level and subcellular distribution pattern of ERECTA-YFP were found (Fig. 1K). However, prolonged treatment for 48 hours resulted in an increase of interior ERECTA-YFP fluorescence signals (Fig. 1L, M).

Immunoblotting results confirmed the increase of ERECTA protein abundance in TM-treated ERECTA-FLAG transgenic plants (Fig. 1N). However, the large portion of ERECTA-FLAG proteins from the TM-treated plants displayed a faster mobility, which might be due to the increase of newly synthesized proteins with defective protein glycosylation. Since the *ERECTA-FLAG* expression was driven by 35S promoter, we examined the transcription of *ERECTA* gene in non-transgenic wild-type plants. But no significant change of *ERECTA* transcriptional level was found after TM treatment (Fig. S1A).

Thus, the enhanced protein abundance of ERECTA-FLAG in TM-treated plants might be caused by increased protein synthesis or reduced protein degradation. Then, ERECTA-FLAG seedlings were co-treated with TM and Cycloheximide (CHX), a protein synthesis inhibitor, or MG-132, a widely used protein degradation inhibitor that could repress the activity of 26S proteasome. According to immunoblotting results, the abundance of ERECTA-FLAG protein was significantly reduced by CHX. The TM-induced protein accumulation was abolished as well by CHX (Fig. S1I). Inhibition of protein degradation by MG-132 caused an increase of ERECTA-FLAG protein amount. However, combination of TM and MG-132 conferred a stronger accumulation of ERECTA-FLAG proteins (Fig. S1J). Above results indicated that the TM-induced increase of ERECTA protein abundance was mainly caused by the increased protein synthesis instead of reduced degradation. Similarly, the enhanced accumulations of proteins in TM-treated ERL1-FLAG and ERL2-FLAG plants were due to the increased protein synthesis (Fig. 1T; Fig. S1K-N).

To further analyze the glycosylation status of ERECTA protein, Endoglycosidase H (Endo-H) enzyme, which primarily cleaves off N-linked glycans of ER-localized proteins but not the complex glycans of proteins that transported into the Golgi apparatus and further in the secretory pathway, was used to digest the proteins extracted from ERECTA-FLAG transgenic plants (Jin et al., 2007; Nekrasov et al., 2009; Qi et al., 2020). In control plants (DMSO mock), two bands that can be detected by anti-FLAG antibodies after Endo-H digestion in immunoblotting analysis, a lower band (N-glycans removed) and an upper band (non-cleaved protein), indicating that ERECTA protein was partially retained in the ER. However, in TM-treated ERECTA-FLAG plants, the upper band was barely detected after Endo-H digestion, suggesting that TM greatly enhanced the retention of ERECTA protein in the ER (Fig. 1O; S1D).

ERL1:ERL1-YFP mainly localized at the PM and partially appeared in the endosomes of stomatal precursor cells (Fig. 1P, R) (Qi et al., 2020). Interestingly, unlike ERECTA-YFP, ERL1-YFP showed significant accumulation in the ring-like structure after TM treatment (Fig. 1Q, S). *ERL2:ERL2-YFP* exhibited the punctate and PM localization in stomatal lineage cells (Ho et al., 2016). Like ERL1-YFP, ERL2-YFP signals accumulated in the ring-like structure after TM treatment as well (Fig. S1F, G). Similar to ERECTA-FLAG, both ERL1-FLAG and ERL2-FLAG from TM-treated plants were hypersensitive to Endo-H digestion (Fig. 1U; Fig. S1E, H).

In addition, we examined the effect of TM on YFP-tagged SERK3 and GFP-tagged BRI1, which are PM-localized receptors and also have functions in stomatal development (Meng et al., 2015; Kim et al., 2012). However, after 48 hours of TM treatment, no obvious changes in their expression level and subcellular localization were found for both SERK3-YFP and BRI1-GFP (Fig. S1O-R). Taken together, our results suggested that the protein N-glycosylation affects protein biogenesis, subcellular localization, and function of ERECTAf receptors in stomatal development.

Dysfunction of ER-resident chaperone complex reduces the abundance but not subcellular dynamics of ERECTA

ERdj3B is the core component of SDF2-ERdj3B-BiP complex, but none of the three *ERECTAf* genes showed significant changes in *erdj3b-1* mutant at the transcription levels (Fig. S2). Then we determined the total protein abundance of the ERECTAf receptors in the *erdj3b-1* mutant by using rabbit polyclonal antibodies that recognize all three ERECTAf members. The total protein levels of ERECTAf were 60% lower in *erdj3b-1* mutant than that in wild-type plants (Fig. 2A).

To further narrow down if individual ERECTAf members were differentially affected in *erdj3b-1*, by using the same antibodies, we evaluated the total ERECTAf proteins amount in different combinations of *ERECTAf* double

mutants, each would contain the third family member intact in the genome. We found that a dramatic reduction of protein abundance in *erdj3b-1 erl1-5 erl2-3*, compared with *erl1-5 erl2-3* (Fig. 2B). By contrast, the total protein amounts in *erdj3b-1 er-105 erl1-5* and *erdj3b-1 er-105 erl2-3* were slightly changed compared with that in *er-105 erl1-5* and *er-105 erl2-3*, respectively (Fig. 2C, D). These results suggested that the lowered total protein level of ERECTAf receptor proteins in *erdj3b-1* is mainly caused by the decrease of ERECTA, rather than of ERL1 or ERL2.

Then, we investigated whether the *erdj3b* mutation affects subcellular localizations of the ERECTAf receptors. ERECTA-YFP (*er-105* complementary) was colocalized with the styryl dye FM4-64 at the PM (Fig. 2E). Consisting with the immunoblotting results, the overall fluorescence intensity of ERECTA-YFP in *erdj3b-1* was dramatically reduced, especially at the PM (Fig. 2F). In addition, the reduced expression level of ERECTA-YFP was also observed in the other chaperone mutant *sdf2-2* (Fig. S3), suggesting that the involvement of SDF2-ERdj3-BiP complex in maintaining the protein abundance of ERECTA.

Kifunensine (Kif) is an inhibitor of ER α-mannosidase that would prevent protein degradation via the ERAD pathway (Huttner et al., 2014; Chen et al., 2020). The expression of ERECTA-YFP (*er-105* complementary) was significantly enhanced by Kif or MG-132 (Fig. 2G-I). However, these effects were completely abolished in *erdj3b-1* mutant (Fig. 2J-L), supported by the quantitative analysis of ERECTA-YFP fluorescent intensities in stomatal lineage cells (Fig. 2M). Collectively, our results indicated that SDF2-ERdj3B-BiP complex was involved in the modulation of ERECTA protein abundance.

To test the possible influence of the *erdj3b-1* mutation on intracellular trafficking of ERECTA-YFP, we used Brefeldin A (BFA), an inhibitor of ADP-ribosylation factor guanine-nucleotide exchange factors (Geldner et al., 2003; Lanhans et al., 2011; Naramoto et al., 2014; Qi et al., 2020). Application of 50 μM BFA for 1 h resulted in aggregation of ERECTA-YFP in “BFA-body”

structures. After 1 h water wash-out, the BFA-bodies disappeared and ERECTA-YFP relocated to the PM (Fig. 2N-P; S4). Although the expression level of ERECTA-YFP in *erdj3b-1* is lower than that in the wild-type, the response of ERECTA-YFP to BFA treatment in *erdj3b-1* is similar to those in the wild-type (*er-105* complementary), indicating that the *erdj3b* mutation has no discernible consequence on the intracellular trafficking of ERECTA (Fig. 2Q-S).

The chaperone complex is required for the subcellular dynamics of ERL1 and ERL2

ERL1:ERL1-YFP (*erl1-5* complementary) displayed a predominant localization at the PM (Fig. 3A). In *erdj3b-1* mutant background, ERL1-YFP exhibited a ring-like structure surrounding the nucleus (Fig. 3B). Results of quantitative image analysis demonstrated that, in the *erl1-5* stomatal precursor cells, ERL1-YFP displayed partial colocalization with an ER marker mCherry-HDEL (Fig. 3C). But, in *erdj3b-1* precursor cells, ERL1-YFP highly colocalized with mCherry-HDEL in close proximity to the nucleus (Fig. 3D). Meanwhile, the fluorescence level of ERL1-YFP was decreased at the PM, which was labelled by FM4-64 dyes (Fig. 3E, F). The ER-retention of ERL1-YFP in *erdj3b-1* is recapitulated in *sdf2-2* mutant (Fig. S5A, B), suggesting that the functional SDF2-ERdj3B-BiP chaperone complex is required for the transport of ERL1 protein from ER to PM.

To further check the effects of *erdj3b-1* mutation on ERL1 retention in the ER, we performed Endo-H assay using the ERL1-FLAG proteins extracted from *erdj3b-1* plants. In contrast to the two bands with similar intensity in wild-type ERL1-FLAG plants, *erdj3b-1* mutant produced a stronger lower band of ERL1-FLAG (cleaved protein) after Endo-H digestion, demonstrating that *erdj3b-1* mutation induced an increased portion of ERL1-FLAG remained in the ER (Fig. 3G). By contrast, the ERECTA-FLAG proteins extracted from wild-type and *erdj3b-1* plants showed a similar sensitivity to Endo-H digestion

(Fig. S5C), indicating the distinct effects of *erdj3b-1* mutation on ERL1 and ERECTA.

We also monitored the BFA responses of ERL1-YFP in *erdj3b-1* mutant. In the epidermis of *erl1-5* precursor cells, ERL1-YFP was sensitive to 50 μM BFA treatment by forming the "BFA-bodies" (Fig. 3H, I). However, ERL1-YFP in *erdj3b-1* mutant failed to colocalized with FM4-64 in the "BFA-bodies" (Fig. 3J, K). Wortmannin (Wm), which could cause a fusion of MVB/LEs by inhibiting phosphatidylinositol-3 (PI3) and phosphatidylinositol-4 (PI4) kinases (Foissner et al., 2016; Qi et al., 2020), was found to induce the dilation of late endosomal ERL1-YFP signals (Fig. 3L, M). However, the formation of such dilated ERL1-YFP-positive "Wm-bodies" was suppressed in *erdj3b-1* (Fig. 3N, O). Above results suggested that the defective transport of ERL1 to PM via the secretion pathway in *erdj3b-1* might lead to a reduction of PM-localization and consequent internalization of ERL1.

ERL2-YFP in *erdj3b-1*, like ERL1-YFP, lost its predominant localization at the PM and accumulated mostly in the ER (Fig. S5D, E). Consistently, ERL2-FLAG proteins extracted from *erdj3b-1* plants displayed hypersensitive to Endo-H treatment (Fig. S5F). Therefore, ER-resident chaperone complex SDF2-ERdj3B-BiP modulates ERECTAf receptors in distinct manners, *i.e.* by affecting the protein abundance for ERECTA versus the subcellular dynamics for ERL1 and ERL2.

The BRI1, TMM, and the auxin transporters AUX1 and PIN3 are also involved in stomatal development (Nadeau and Sack, 2002; Kim et al., 2012; Le et al., 2014). However, none of them exhibited visible changes in the *erdj3b-1* stomatal lineage cells (Fig. S6). The impacts of SDF2-ERdj3B-BiP on ERECTAf receptors seemed to be not a universal phenomenon.

Genetic relationship of chaperone complex with ERECTAf receptors in regulating stomatal development

Compared with wild type, no obvious stomatal phenotypes were observed in *erdj3b-1* mutant leaf epidermis (Fig. 4A, B). As reported previously, *er-105* produced excessive arrested stomatal lineage cells that were unable to differentiate into mature stomata (Fig. 4C, K, colored in pink) (Shpak et al., 2005). However, the additional *erdj3b* mutation in *er-105* reduced the percentage of small precursor-like cells (PrCs, over the total number of PrCs and mature stomata) and induced stomatal clusters, leading to an increased stomatal density. Similar phenotypes were also found in *sdf2-2 er-105* mutant, confirming the requirement of functional SDF2-ERdj3B-BiP complex in stomatal development (Fig. S7A-F). Introduction of the *ERdj3B-GFP* restored the appearance of small precursor-like cells in *erdj3b-1 er-105* epidermis (Fig. S7G, H). ERdj3B-GFP highly colocalized with the ER marker mCherry-HDEL, supporting that ERdj3B, as predicated, is an ER-resident molecular chaperone (Fig. S7I, J).

Mutation of *erl1* was able to resume the stomatal precursor cell differentiation in *er-105* (Fig. 4E) (Shpak et al., 2005). However, comparing with *er-105 erl1-5*, the *erdj3b-1 er-105 erl1-5* triple mutant exhibited more severe stomatal clustering phenotype and increased number of mature stomata (Fig. 4F, K), indicating that the *erdj3b* mutation caused the dysfunction of other regulator (s), like ERL2, besides ERECTA and ERL1.

In contrast to function of *erl1* mutation, additional *erl2* mutation enhanced the formation of excessive PrCs in *er-105* mutant (Fig. 4G, L). The *erdj3b-1 er-105 erl2-3* triple mutant displayed a reduced percentage of PrCs, comparing with *er-105 erl2-3* double mutant (Fig. 4H, L). We suspected that the action of ERdj3B is possibly through ERL2, which is antagonistic to ERL1 in repressing the precursor cell differentiation. However, *erl1-5 erl2-3* displayed normal stomatal development (Fig. 4I). No observable change of stomatal phenotype was found in *erdj3b-1 erl1-5 erl2-3* mutant (Fig. 4J),

suggesting the redundant function of ERECTA in stomatal development control, though the abundance of ERECTA receptors was reduced due to the *erdj3b-1* mutation. Furthermore, we checked the impacts of *erdj3b-1* mutation on stomatal development in the hypocotyl, where TMM acts to dampen the ERECTAf-mediated signaling (Shpak et al., 2005). In agreement with the statement that ERdj3B functions in stomatal differentiation, mutaton of *erdj3b-1* confered stomatal production in *tmm-1* hypocotyls, mimicking the stomatal phenotype in *tmm-1 erl1-5* mutant hypocotyls (Fig. 4M-Q).

The YODA (YDA) MAPK cascade acts downstream of the TMM-ERECTA receptor complexes in stomatal development (Lampard et al., 2008; Lampard et al., 2014). Notably, the *erdj3b-1* mutation neither affected the excessive stomatal phenotype of loss-of-function *yoda* mutant, nor altered the stomata-less phenotypes of the constitutively active *CA-YDA* plants (Fig. 5A-D, M), indicating that *ERdj3B* genetically functions upstream of the YODA-MAPK cascade. Loss of BASL function in *basl-2* allele induced the formation of clustered precursor-like cells in epidermis (Dong et al., 2009; Zhang et al., 2015) (Fig. 5E). However, the *erdj3b-1* mutation failed to convert these small precursor-like cells into mature stomata, indicating that ERdj3B is unlikely to act in a same pathway with BASL (Fig. 5F, M, N). On the contrary, the stomatal phenotypes induced by overexpression of *EPF1*, *EPF2*, or *EPFL9/Stomagen* were abolished or reduced in *erdj3b-1* mutant background (Fig. 5G-N), further confirming a role of ERdj3B in ERECTAf receptor-mediated signaling during stomatal development.

DISCUSSION

The functions of secretory EPF/EPFL peptides and TMM-ERECTAf receptors in *Arabidopsis* stomatal development have been intensively investigated (Yang and Sack, 1995; Shpak et al., 2005; Hara et al., 2007; Hunt and Gray, 2009; Dong and Bergmann, 2010; Pillitteri and Torii, 2012; Qu

et al., 2017). Three ERECTAf receptors redundantly govern the initial decision of stomatal lineage and distribution pattern in epidermis, but individual members contribute differently to the stomatal lineage cell differentiation. A raised question is what determines the distinct roles of ERECTAf receptors with high homology.

In eukaryotic cells, the majority of membrane receptor proteins are processed in the ER and controlled by the ERQC system. Only correctly folded receptors can exit from the ER and be transported to their final PM destination via the secretory pathway. Improperly or incompletely folded proteins are retained in the ER for further folding or ultimately degraded by ERAD (Fig. 6). Several conserved N-glycosylation motifs like N(X)S/T have been predicted in the ectodomain (LRR) of the ERECTAf receptors (Chakraborty et al., 2019). Here, we experimentally confirmed that inhibition of protein N-glycosylation by TM significantly affects the protein abundance and subcellular distribution of all three ERECTAf receptors. Whether the N-glycosylation differences cause the functional diversities of ERECTA family receptors needs to be further investigated. However, we found that the dysfunction of ER-resident chaperone complex of SDF2-ERdj3B-BiP differentially affects the biogenesis and subcellular dynamics of ERECTAf receptors.

ERECTA is broadly expressed in the epidermis and plays a predominant role overlapping with ERL1 and ERL2 in stomatal pattering control. In contrast to the normal stomatal phenotypes of *erl1*, *erl2*, *erl1 erl2*, the single mutation of *erecta* confers an increase of stomatal lineage cells. Although the abundance of ERECTA is reduced in *erdj3b* mutant, the intracellular trafficking of the remained ERECTA protein is normal. Additional mutation of *erdj3b* has no impacts on *erl1 erl2* stomatal phenotype is due to the presence of functional ERECTA. This functional insensitivity of ERECTA, unlike ERL1 and ERL2, to dysfunction of chaperone complex, maintains a minimum signaling that enforces the stomatal “one-cell-spacing” rule.

We found that the transcriptional level of ERECTA was not altered by *erdj3b* mutation. The effects of Kif and MG-132 on the abundance of ERECTA in *erdj3b-1* mutant is limited, suggesting the reduction of ERECTA proteins is mainly caused by the down-regulation of protein synthesis, but not the protein degradation (Fig. 6). Similarly, the protein level of EFR, also a leucine-rich repeat receptor kinase, in total extracts was strongly reduced in the *sdf2-2* backgrounds, though the transcription of *EFR* was not changed (Nekrasov et al., 2009). Accumulation of misfolded proteins in the ER triggers the unfolded protein response (UPR). In yeast and mammalian cells, the UPR leads to a halt of protein synthesis through the action of Protein Kinase RNA-like Endoplasmic Reticulum Kinase (PERK). The release of BiP from PERK results in PERK autophosphorylation and subsequently inhibits the protein translation via the phosphorylation of eIF2α, the key translation initiation factor. *Arabidopsis* has eIF2α but no PERK homolog has been found. In response to the Dithiothreitol (DTT)-induced ER stress, General Control Nonderepressible1 (GCN1) and GCN2 promote the phosphorylation of eIF2α (Izquierdo et al., 2018). In maize, ER-stress induces the decline of protein translation efficiency because the sequestration of mRNAs in stress granules (Kanodia et al, 2020). Therefore, in response to ER stress, like yeast and mammalian cells, plants have ways to relieve the protein overload in the ER by down-regulating the general protein synthesis.

Both ERL1 and ERL2 are specifically expressed in stomatal lineage cells and exhibit hypersensitivity to ER stress. It was demonstrated that EPF1-induced ERL1 internalization and trafficking, in which TMM is essential, are required for the function of ERL1 in restricting stomatal lineage cell differentiation. While EPFL9/Stomagen competes with EPF1 by trigging the retention of ERL1 in the ER (Qi et al., 2020). In agree with this, the arrested stomatal differentiation in *erecta* leaves and *tmm* hypocotyls are rescued in *erdj3b-1* mutant background. In addition, the effects of *EPF1* and *EPFL9/Stomagen* overexpression on stomatal phenotypes are abolished in

erdj3b-1 mutant, further supporting that ER-resident molecular chaperones are required for the subcellular dynamics and function of ERL1.

ERL2, like TMM, can heteromerized with ERECTA and ERL1 to modulate signaling through the interaction with VST protein at ER-PM contact sites (Ho et al., 2016). Here, we provide evidence that ERL2 localization and function are modulated by SDF2-ERdj3B-BiP. Additional *erdj3b* mutation in *erecta erl1* produced excessive stomata in clusters, resembling the phenotypes of *erecta erl1 erl2* triple mutant. Mutation of *erdj3b* caused the majority of ERL1 protein retained in the ER and failed to transport to the PM, consequently alleviated the repressing effect of ERL1 on stomata lineage cell differentiation in *erecta erl2* double mutants. The study of molecular chaperone complex SDF2-ERdj3B-BiP as a modulator of ERECTAf receptors in the ER will be helpful to further reveal the fine-tune mechanism of stomatal patterning and development.

MATERIALS AND METHODS

Plant materials and growth conditions

Arabidopsis accession Columbia (Col-0) was used as wild-type. The *erdj3b-1* (SALK_113364), *erl1-5* (SALK_019567), *erl2-3* (GK_486E03) and *sdf2-2* (SALK_141321) were ordered from *Arabidopsis* Biological Resource Center (ABRC, https://abrc.osu.edu). The following higher-order mutants and marker lines were generated by crossing: *erdj3b-1 er-105*, *er-105 erl2-3*, *erdj3b-1 er-105 erl2-3*, *er-105 erl1-5*, *erdj3b-1 er-105 erl1-5*, *erl1-5 erl2-3*, *erdj3b-1 erl1-5 erl2-3*, *erdj3b-1 tmm-1*, *sdf2-2 er-105*, *erdj3b-1 yoda*, *erdj3b-1 CA-YDA*, *erdj3b-1 basl-2*, *ERECTA:ERECTA-YFP erdj3b-1*, *ERECTA:ERECTA-YFP sdf2-2*, *ERL1:ERL1-YFP erdj3b-1*, *ERL1:ERL1-YFP 35S:mCherry-HDEL*, *ERL1:ERL1-YFP 35S:mCherry-HDEL erdj3b-1*, *ERL1:ERL1-YFP sdf2-2*, *ERL2:ERL2-YFP erdj3b-1*, *ERdj3B:ERdj3B-GFP 35S:mCherry-HDEL*, *PIN3:PIN3-GFP erdj3b-1*, *AUX1:AUX1-YFP erdj3b-1*,

and *BRI1:BRI1-GFP erdj3b-1*, *SUPER:ERECTA-FLAG erdj3b-1*, *SUPER:ERL1-FLAG erdj3b-1*, *SUPER:ERL2-FLAG erdj3b-1*, *ERdj3B:ERdj3B-GFP 35S:mCherry-HDEL*. Sterilized seeds were grown on half strength of Murashige and Skoog (1/2 MS) medium supplemented with 1% sucrose and 0.8% agar at 22°C in a growth room with a 16 h light/ 8 h dark light regime.

Plasmid construction and plant transformation

To obtain *ERdj3B:ERdj3B-GFP*, the full-length genomic DNA of *ERdj3B* without T-Nos driven by its native promoter was cloned into pCAMBIA1300-GFP vector (Cambia). For *SUPER:ERECTA-FLAG*, *SUPER:ERL1-FLAG* and *SUPER:ERL2-FLAG*, the full-length genomic DNA of *ERECTA*, *ERL1*, and *ERL2* without T-Nos was cloned into pCAMBIA1300-FLAG vector (Cambia), respectively. For *ERECTA:ERECTA-YFP*, *ERL1:ERL1-YFP*, *ERL2:ERL2-YFP*, *SERK3:SERK3-YFP* constructs, the genomic coding regions of *ERECTA*, *ERL1*, *ERL2*, and *SERK3* (from ATG to immediately ahead of the stop codon) were amplified and cloned into pENTR/D-TOPO (Invitrogen), respectively. Next, the promoter regions were amplified and inserted into the Not I site of the pENTR/D-TOPO carrying genomic regions, respectively. Then, the entry clone was recombined by the Clonase II enzyme mix (Invitrogen) into the destination vector pHGY for expression in plants. To obtain *35S:EPF1*, *35S:EPF2*, and *35S:EPFL9* constructs, the cDNA of *EPF1*, *EPF2*, and *EPFL9* fragments were obtained by PCR amplification. Then the fragments were cloned into a pCAMBIA1300 vector under control of 35S promoter. Primers used for plasmid constructs were listed in Table S1. All constructs were transformed into *Agrobacterium tumefaciens* strain EHA105, and then transformed into wild-type or *erdj3b-1* mutant seedlings by floral dipping. Transgenic plants were selected on 1/2 MS medium containing 25 μg/mL hygromycin.

RT-qPCR

Total RNA from 5-day-old wild-type, and *erdj3b-1* seedlings were extracted using HiPure Plant RNA Mini Kit (Magen). Reverse transcription was performed using PrimeScript RT reagent Kit (TaKaRa). Amplified *ACTIN2* gene was used as an internal control. Real-time quantitative PCR experiments were repeated independently for three times. The data were averaged, and cDNA was amplified using Hieff® qPCR SYBR Green Master Mix (Yeasen) with Roche Applied Science Light Cycler 96. Primers specific to target genes used for quantitative RT-PCR are listed in the Table S1.

Immunoblotting analysis

For ERECTAf endogenous proteins analysis, the peptide containing amino acids 25-332 of the ERECTA protein sequence was used to produce an ERECTA family-specific rabbit polyclonal antibody (Abmart, Shanghai, China). Total proteins were extracted from etiolated 4-day-old seedlings of Col-0, *erdj3b-1*, *er-105 erl1-5*, *erdj3b-1 er-105 erl1-5*, *er-105 erl2-3*, *erdj3b-1 er-105 erl2-3*, *erl1-5 erl2-3*, *erdj3b-1 erl1-5 erl2-3* using protein extraction buffer, 100 mM Tris-HCl at pH 7.5, 150 mM NaCl, 2 mM EDTA, 2% TritonX-100, 20% glycerol, 20 mM NaF, 1 mM Phenylmethanesulfonyl fluoride (PMSF), 1X protease inhibitor cocktail (Roche). Homogenate was centrifuged at 5,000 *g* for 30 min to remove debris. Supernatants used for immunoblotting analysis using anti-ERECTA-family antibody (1:5,000). Actin is used as loading control detected by anti-Actin antibody (1:5,000).

For TM, CHX or MG-132 treatment, *SUPER:ERECTA-FLAG*, *SUPER:ERL1-FLAG*, and *SUPER:ERL2-FLAG* seedlings were first grown on 1/2 MS medium plates for 2 days, and then treated with 60 ng/mL TM or combination with 100 μM CHX or 40 μM MG132 for 48 hours. The total proteins were extracted as descried above. Supernatants used for

immunoblotting analysis. Anti-FLAG antibody (1:10,000) and anti-Actin antibody (1:5,000) were used in immunoblot analysis.

Endo-H enzymatic assay

Total proteins were extracted from 4-day-old seedlings of *SUPER:ERECTA-FLAG*, *SUPER:ERECTA-FLAG erdj3b-1*, *SUPER:ERL1-FLAG*, *SUPER:ERL1-FLAG erdj3b-1*, *SUPER:ERL2-FLAG*, *SUPER:ERL2-FLAG erdj3b-1*. For TM treatment, *SUPER:ERECTA-FLAG*, *SUPER:ERL1-FLAG*, and *SUPER:ERL2-FLAG* seedlings were first grown on 1/2 MS medium plates for 2 days, and then treated with 0.01% DMSO or 60 ng/mL TM for 48 hours. Extracted proteins were digested with Endo-H (NEB) for 5-60 min at 37˚C before immunoblot analysis. Anti-FLAG antibody (1:10,000) and anti-Actin antibody (1:5,000) were used in immunoblot analysis.

Microscopy and image analysis

To obtain Differential Interference Contrast (DIC) images, cotyledons or hypocotyls were cleared with a destaining solution (containing 75% ethanol and 25% acetic acid) for overnight at room temperature. After a treatment with basic solution (7% NaOH in 60% ethanol) for 15 min at room temperature, the samples were rehydrated via an ethanol series (40%, 20%, and 10%) for 20 min at each step. Images were captured using an Olympus BX51 microscope.

For FM4-64 (Invitrogen) staining, cotyledons of 4-day-old seedlings of *ERECTA:ERECTA-YFP*, *ERECTA:ERECTA-YFP erdj3b-1*, *ERL1:ERL1-YFP*, *ERL1:ERL1-YFP erdj3b-1* were immersed into 2 μM FM4-64 for 30 min. For propidium iodide staining, cotyledons of 4-day-old seedlings were stained with 0.1% propidium iodide for 1 min. Confocal images were captured using a laser scanning confocal microscope Olympus FV1000-MPE. The excitation/emission spectra are 488 nm/501-528 nm for GFP/YFP fluorescent proteins, and 543 nm/600-620 nm for mCherry, FM4-64, and propidium iodide.

The line scan across the stomatal precursor cells were analyzed with Plot Profile function of ImageJ (https://imagej.nih.gov/ij/).

Pharmacological treatment

To assess the impacts of TM on stomatal development, 10-day-old seedlings grown in 1/2 MS medium supplemented with 30 ng/mL, 60 ng/mL, 120 ng/mL, and 240 ng/mL TM (Macklin) were used. 2-day-old *ERECTA:ERECTA-YFP er-105*, *ERL1:ERL1-YFP erl1-5*, *ERL2:ERL2-YFP*, *SERK3:SERK3-YFP*, and *BRI1:BRI1-GFP* seedlings were treated with 60 ng/mL tunicamycin for 24 or 48 hours before imaging.

For Kifunensine or MG-132 treatment, 3-day-old seedlings of *ERECTA:ERECTA-YFP* and *ERECTA:ERECTA-YFP erdj3b-1* were treated with 20 μM Kifunensine (MCE) or 40 μM MG-132 (Merck) for 12 hours.

For BFA treatment, 4-day-old seedlings were first immersed into 2 μM FM4-64 for 30 min before treatment of 50 μM BFA solution (Macklin) for 60 min. For BFA wash-out, seedlings were rinsed in water for 60 min.

For wortmannin treatment, *ERL1:ERL1-YFP erl1-5* and *ERL1:ERL1-YFP erdj3b-1* seedlings were treated with 25 μM wortmannin (Selleck) for 10 min before imaging.

Quantification and statistical analysis

For quantitative analysis of relative protein abundance of ERECTAf receptors, the mean gray value of bands recognized by anti-ERECTAf antibodies in immunoblots were measured using ImageJ. The relative ratios of mean gray value of bands were used in the pairwise comparison of protein abundance. Data represented the one of three independent experiments.

For the quantitative analysis of the effects of Kifunensine or MG-132 on ERECTA-YFP expression, the mean intensity values of YFP fluorescence from stomatal precursor cells were measured using ImageJ. Data are from one experiment representative of three independent experiments.

For quantitative analysis of *Arabidopsis* stomatal phenotypes, the numbers of mature stomata and precursor-like cells (PrCs) in a region of 0.2 mm^2 from the same quadrant of 12 adaxial cotyledons were scored. Small epidermal cells with area size equal or smaller than a normal stomatal guard mother cell was classified as PrCs (Le et el., 2014). The PrCs percentage are the number of PrCs over the total number of PrCs and mature stomata.

All statistical analyses were conducted with SPSS 25.0 software. To compare two normally distributed groups, *F*-tests were performed first, and then unpaired two-tailed *t*-tests were used. For multiple comparisons between normally distributed groups, one-way analysis of variance (ANOVA) followed by Tukey's post-hoc test was used.

Acknowledgement

We thank Prof. Zu-Hua He (CAS Center for Excellence in Molecular Plant Sciences, Chinese Academy of Sciences, Shanghai, China) for the gifts of *er-105* mutant seeds. Prof. Wei-Cai Yang (Institute of Genetics and Developmental Biology, Chinese Academy of Sciences, Beijing, China) for the gift of mCherry-HDEL plasmid. We thank Wei Wang for his critical reading and English editing (Swedish University of Agricultural Sciences, Sweden). We thank Jing-Quan Li from Plant Science Facility of the Institute of Botany, Chinese Academy of Sciences for her excellent technical assistance of Confocal analysis.

Competing interests

The authors declare no competing or financial interests.

Author contributions

K.Z.Y., L.Q.C., and J.L. designed the research and analyzed the data. K.Z.Y., C.R.Z., Y. J.L., and X.Y.X. performed most of the experiments. H.C.L. and Z.B.F. contributed to the data analysis. K.Z.Y., J.D., and J.L. wrote the article.

Funding

This work was supported by grants from the National Natural Science Foundation of China program 31871377 and 32070723 (K.Z.Y.), 31970804 and 32170722 (J.L.), 31470279 and 31872668 (L.Q.C.).

References

Abrash, E. B., Davies, K. A. and Bergmann, D. C. (2011). Generation of signaling specificity in *Arabidopsis* by spatially restricted buffering of ligand-receptor interactions. *Plant Cell* **23**, 2864-2879. doi:10.1105/tpc.111.086637

Bhave, N. S., Veley, K. M., Nadeau, J. A., Lucas, J. R., Bhave, S. L. and Sack, F. D. (2009). TOO MANY MOUTHS promotes cell fate progression in stomatal development of *Arabidopsis* stems. *Planta* **229**, 357-367. doi:10.1007/s00425-008-0835-9

Buchberger, A., Bukau, B. and Sommer, T. (2010). Protein quality control in the cytosol and the endoplasmic reticulum: brothers in arms. *Mol. Cell* **40**, 238-252. doi:10.1016/j.molcel.2010.10.001

Chakraborty, S., Nguyen, B., Wasti, S. D. and Xu, G. (2019). Plant Leucine-Rich Repeat Receptor Kinase (LRR-RK): structure, ligand perception, and activation mechanism. *Molecules* **24**, 3081. doi:10.3390/molecules 24173081

Chen, T., Zhang, H., Niu, G., Zhang, S. and Hong, Z. (2020). Multiple N-glycans cooperate in balancing misfolded BRI1 secretion and ER retention. *Plant Mol. Biol.* **103**, 581-596. doi:10.1007/s11103-020-01012-z

Dong, J., MacAlister, C. A. and Bergmann, D. C. (2009). BASL controls asymmetric cell division in *Arabidopsis*. *Cell* **137**, 1320-1330. doi:10.1016/j.cell.2009.04.018

Dong, J. and Bergmann, D. C. (2010). Stomatal patterning and development. *Curr. Top. Dev. Biol.* **91**, 267-297. doi:10.1016/s0070-2153(10)91009-0

Foissner, I., Sommer, A., Hoeftberger, M., Hoepflinger, M. C. and Absolonova, M. (2016). Is Wortmannin-Induced reorganization of the trans-Golgi network the key to explain charasome formation? *Front Plant Sci*. **7**, 756. doi:10.3389/fpls.2016.00756

Geldner, N., Anders, N., Wolters, H., Keicher, J., Kornberger, W., Muller, P., Delbarre, A., Ueda, T., Nakano, A. and Jurgens, G. (2003). The *Arabidopsis* GNOM ARF-GEF mediates endosomal recycling, auxin transport, and auxin-dependent plant growth. *Cell* **112**, 219-230. doi:10.1016/s0092-8674(03)00003-5

Hara, K., Kajita, R., Torii, K. U., Bergmann, D. C. and Kakimoto, T. (2007). The secretory peptide gene EPF1 enforces the stomatal one-cell-spacing rule. *Genes Dev.* **21**, 1720-1725. doi:10.1101/gad.1550707

Helenius, A. and Aebi, M. (2004). Roles of N-linked glycans in the endoplasmic reticulum. *Annu. Rev. Biochem.* **73**, 1019-1049. doi:10.1146/annurev.biochem.73.011303.073752

Ho, C. M., Paciorek, T., Abrash, E. and Bergmann, D. C. (2016). Modulators of stomatal lineage signal transduction alter membrane contact sites and reveal specialization among ERECTA kinases. *Dev. Cell* **38**, 345-357. doi:10.1016/j.devcel.2016.07.016

Hong, Z., Kajiura, H., Su, W., Jin, H., Kimura, A., Fujiyama, K. and Li, J. (2012). Evolutionarily conserved glycan signal to degrade aberrant brassinosteroid receptors in *Arabidopsis*. *Proc. Natl. Acad. Sci. U.S.A.* **109**, 11437-11442. doi:10.1073/pnas.1119173109

Hunt, L. and Gray, J. E. (2009). The signaling peptide EPF2 controls asymmetric cell divisions during stomatal development. *Curr. Biol.* **19**, 864-869. doi:10.1016/j.cub.2009.03.069

Huttner, S., Veit, C., Vavra, U., Schoberer, J., Dicker, M., Maresch, D., Altmann, F. and Strasser, R. (2014). A context-independent N-glycan signal targets the misfolded extracellular domain of *Arabidopsis* STRUBBELIG to endoplasmic-reticulum-associated degradation. *Biochem. J.* **464**, 401-411. doi:10.1042/BJ20141057

Izquierdo, Y., Kulasekaran, S., Benito, P., López, B., Marcos, R., Cascón, T., Hamberg, M. and Castresana, C. (2018). *Arabidopsis* nonresponding to oxylipins locus NOXY7 encodes a yeast GCN1 homolog that mediates noncanonical translation regulation and stress adaptation. *Plant Cell Environ*. **41**, 1438-1452. doi:10.1111/pce.13182

Jin, H., Yan, Z., Nam, K. H. and Li, J. (2007). Allele-specific suppression of a defective brassinosteroid receptor reveals a physiological role of UGGT in ER quality control. *Mol. Cell* **26**, 821-830. doi:10.1016/j.molcel.2007.05.015

Kanodia, P., Vijayapalani, P., Srivastava, R., Bi, R. and Howell, S. H. (2020). Control of translation during the unfolded protein response in maize seedlings: life without PERKs. *Plant Direct*. **4**, e00241. doi:10.1002/pld3.241

Kim, T. W., Michniewicz, M., Bergmann, D. C. and Wang, Z. Y. (2012). Brassinosteroid regulates stomatal development by GSK3-mediated inhibition of a MAPK pathway. *Nature* **482**, 419-422. doi:10.1038/nature10794

Lampard, G. R., Macalister, C. A. and Bergmann, D. C. (2008). *Arabidopsis* stomatal initiation is controlled by MAPK-mediated regulation of the bHLH SPEECHLESS. *Science* **322**, 1113-1116. doi:10.1126/science.1162263

Lampard, G. R., Wengier, D. L. and Bergmann, D. C. (2014). Manipulation of mitogen-activated protein kinase kinase signaling in the *Arabidopsis* stomatal lineage reveals motifs that contribute to protein localization and signaling specificity. *Plant Cell* **26**, 3358-3371. doi:10.1105/tpc.114.127415

Lanhans, M., Förster, S., Helmchen, G., and Robinson, D.G. (2011). Differential effects of the brefeldin A analogue (6R)-hydroxy-BFA in tobacco and *Arabidopsis*. *J. Exp. Bot.* **62**, 2949-2957. doi:10.1093/jxb/err007

Le, J., Liu, X. G., Yang, K. Z., Chen, X. L., Zou, J. J., Wang, H. Z., Wang, M., Vanneste, S., Morita, M., Tasaka, M. et al. (2014). Auxin transport and activity regulate stomatal patterning and development. *Nat. Commun*. **5**, 3090. doi:10.1038/ncomms4090

Leng, Y. J., Yao, Y. S., Yang, K. Z., Wu, P. X., Zuo, C. R., Luo, J. H., Wang, P., Liu, Y. Y., Zhang, X. Q., Ye, D. et al. (2022). *Arabidopsis* ERdj3B coordinates with ERECTA-family receptor kinases to regulate ovule development and the heat stress response. *Plant Cell* **28**, doi:10.1093/plcell/koac226

Maruyama, D., Sugiyama, T., Endo, T. and Nishikawa, S. (2014a). Multiple BiP genes of *Arabidopsis thaliana* are required for male gametogenesis and pollen competitiveness. *Plant Cell Physiol*. **55**, 801-810. doi:10.1093/pcp/pcu018

Maruyama, D., Yamamoto, M., Endo, T. and Nishikawa, S. (2014b). Different sets of ER-resident J-proteins regulate distinct polar nuclear-membrane fusion events in *Arabidopsis thaliana*. *Plant Cell Physiol*. **55**, 1937-1944. doi:10.1093/pcp/pcu120

Meng, X., Chen, X., Mang, H., Liu, C., Yu, X., Gao, X., Torii, K. U., He, P. and Shan, L. (2015). Differential function of *Arabidopsis* SERK family receptor-like kinases in stomatal patterning. *Curr. Biol*. **25**, 2361-2372. doi:10.1016/j.cub.2015.07.068

Nadeau, J. A. and Sack, F. D. (2002). Control of stomatal distribution on the *Arabidopsis* leaf surface. *Science* **296**, 1697-1700. doi:10.1126/science.1069596

Naramoto, S., Otegui, M. S., Kutsuna, N., de Rycke, R., Dainobu, T., Karampelias, M., Fujimoto, M., Feraru, E., Miki, D., Fukuda, H. et al. (2014). Insights into the localization and function of the membrane trafficking regulator GNOM ARF-GEF at the Golgi apparatus in *Arabidopsis*. *Plant Cell* **26**, 3062-3076. doi:10.1105/tpc.114.125880

Nekrasov, V., Li, J., Batoux, M., Roux, M., Chu, Z. H., Lacombe, S., Rougon, A., Bittel, P., Kiss-Papp, M., Chinchilla, D. et al. (2009). Control of the pattern-recognition receptor EFR by an ER protein complex in plant immunity. *EMBO J*. **28**, 3428-3438. doi:10.1038/emboj.2009.262

Olden, K., Parent, J. B. and White, S. L. (1982). Carbohydrate moieties of glycoproteins. A re-evaluation of their function. *Biochim. Biophys. Acta*. **650**, 209-232. doi:10.1016/0304-4157(82)90017-x

Pillitteri, L. J. and Torii, K. U. (2012). Mechanisms of stomatal development. *Annu. Rev. Plant Biol*. **63**, 591-614. doi:10.1146/annurev-arplant-042811-105451

Qi, X., Yoshinari, A., Bai, P., Maes, M., Zeng, S. M. and Torii, K. U. (2020). The manifold actions of signaling peptides on subcellular dynamics of a receptor specify stomatal cell fate. *eLife* **9**. doi:10.7554/eLife.58097

Qu, X., Peterson, K. M. and Torii, K. U. (2017). Stomatal development in time: the past and the future. *Curr. Opin. Genet. Dev*. **45**, 1-9. doi:10.1016/j.gde.2017.02.001

Shpak, E. D., McAbee, J. M., Pillitteri, L. J. and Torii, K. U. (2005). Stomatal patterning and differentiation by synergistic interactions of receptor kinases. *Science* **309**, 290-293. doi:10.1126/science.1109710

Strasser, R. (2018). Protein quality control in the endoplasmic reticulum of plants. *Annu. Rev. Plant Biol*. **69**, 147-172. doi:10.1146/annurev-arplant-042817-040331

Sugano, S. S., Shimada, T., Imai, Y., Okawa, K., Tamai, A., Mori, M. and Hara-Nishimura, I. (2010). Stomagen positively regulates stomatal density in *Arabidopsis*. *Nature* **463**, 241-244. doi:10.1038/nature08682

Swarup, R., Kargul, J., Marchant, A., Zadik, D., Rahman, A., Mills, R., Yemm, A., May, S., Williams, L., Millner, P., Tsurumi, S., Moore, I., Napier, R., Kerr, I.D., and Bennett, M.J. (2004). Structure-function analysis of the presumptive *Arabidopsis* auxin permease AUX1. *Plant Cell* **16**, 3069-3083. doi:10.1105/tpc.104.024737

Torii, K. U. (2012). Mix-and-match: ligand-receptor pairs in stomatal development and beyond. *Trends Plant Sci*. **17**, 711-719. doi:10.1016/j.tplants.2012.06.013

Yamamoto, M., Maruyama, D., Endo, T. and Nishikawa, S. (2008). *Arabidopsis thaliana* has a set of J proteins in the endoplasmic reticulum that are conserved from yeast to animals and plants. *Plant Cell Physiol*. **49**, 1547-1562. doi:10.1093/pcp/pcn119

Yamamoto, M., Uji, S., Sugiyama, T., Sakamoto, T., Kimura, S., Endo, T. and Nishikawa, S. I. (2020). ERdj3B-Mediated quality control maintains anther development at high temperatures. *Plant Physiol*. **182**, 1979-1990. doi:10.1104/pp.19.01356

Yang, K. Z., Xia, C., Liu, X. L., Dou, X. Y., Wang, W., Chen, L. Q., Zhang, X. Q., Xie, L. F., He, L., Ma, X. et al. (2009). A mutation in *Thermosensitive Male Sterile 1*, encoding a heat shock protein with DnaJ and PDI domains, leads to thermosensitive gametophytic male sterility in *Arabidopsis*. *Plant J*. **57**, 870-882. doi:10.1111/j.1365-313X.2008.03732.x

Yang, M. and Sack, F. D. (1995). The too many mouths and four lips mutations affect stomatal production in *Arabidopsis*. *Plant Cell* **7**, 2227-2239. doi:10.1105/tpc.7.12.2227

Zhang, Y., Wang, P., Shao, W., Zhu, J. K. and Dong, J. (2015). The BASL polarity protein controls a MAPK signaling feedback loop in asymmetric cell division. *Dev. Cell* **33**, 136-149. doi:10.1016/j.devcel.2015.02.022

Figures

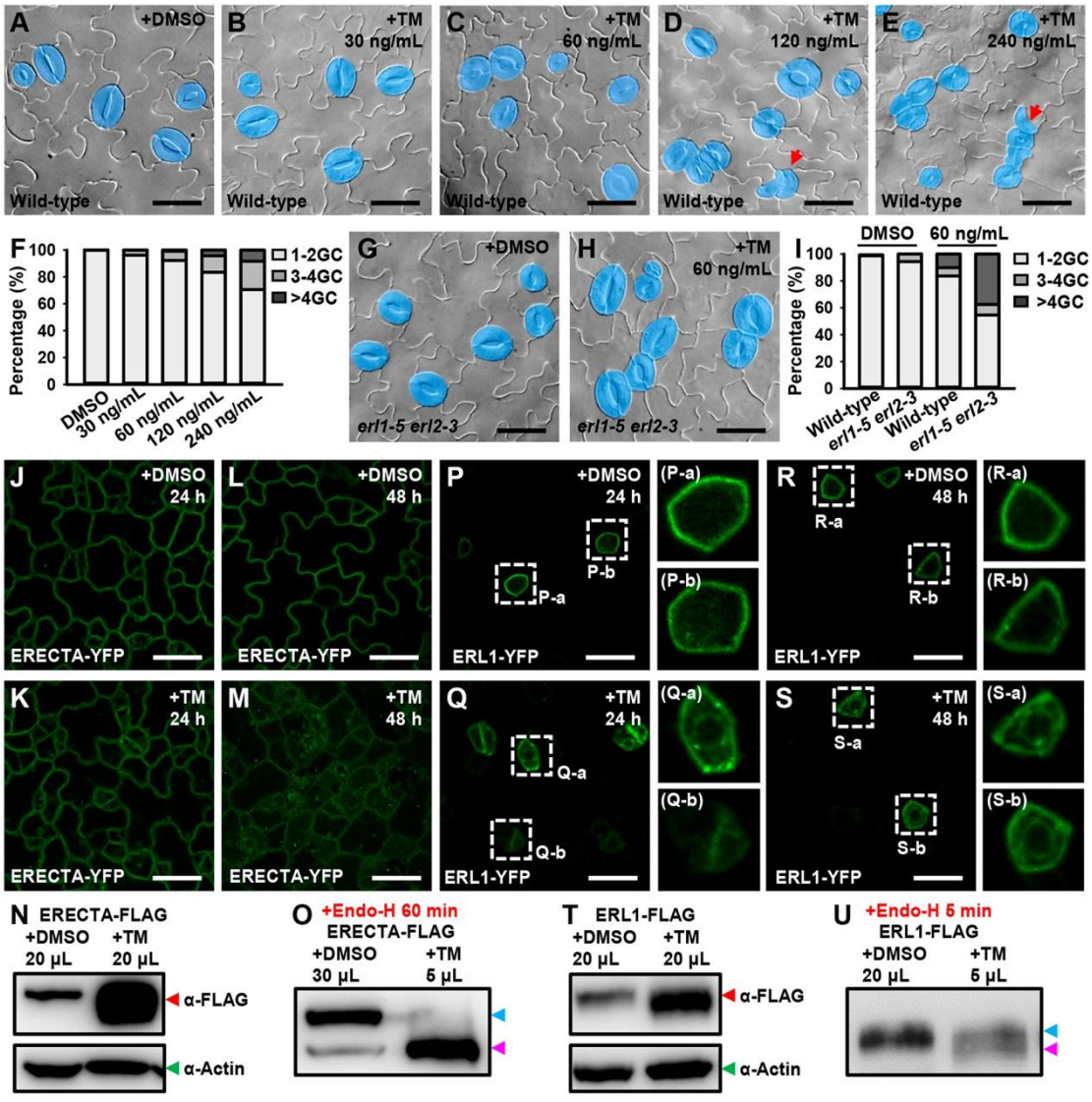

Fig. 1. Response of stomatal development and receptors to tunicamycin-induced ER stress.

(A-E) DIC images of TM-treated wild-type epidermis. TM at 30 ng/mL has no effect on stomatal phenotype, while 60 ng/mL induces stomatal clusters. TM at 120 ng/mL or 240 ng/mL induces more severe clustering phenotypes. GCs are highlighted by blue color. Red arrows, unpaired guard cells within stomatal clusters. (F) Quantification of stomatal phenotypes after treatment of TM at different concentrations. (G-I) *erl1-5 erl2-3* is more sensitive to 60 ng/mL TM

treatment than the wild-type. (J-M) Confocal images of *ERECTA:ERECTA-YFP* in epidermal cells. Reduction of PM-localized ERECTA-YFP expression with an increase of intracellular signals after 48 h TM treatment. (N) Immunoblot analysis indicate an increase of ERECTA-FLAG amount after TM treatment. Top panel, ERECTA-FLAG recognized by anti-FLAG (red arrowhead). Lower panel, the loading control of actin detected by anti-Actin (green arrowhead). (O) Immunoblot analysis of ERECTA-FLAG protein after 60 min digestion with Endo-H. ERECTA-FLAG extracted from TM-treated plants are sensitive to Endo-H. Upper band, non-cleaved proteins (blue arrowhead). Lower band, N-glycans removed proteins (pink arrowhead). See also Fig. S1D. (P-S) Confocal images of *ERL1:ERL1-YFP* expression in stomatal lineage cells. PM and punctate localization of ERL1-YFP are altered after TM treatment. Images at the right, higher magnifications of the regions indicated by white frames. (T) Immunoblot analysis show an increase of ERL1-FLAG amount after TM treatment (red arrowhead). (U) Immunoblot analysis of ERL1-FLAG protein after 5 min digestion with Endo-H. ERL1-FLAG protein extracted from TM-treated plants is sensitive to Endo-H digestion. See also Fig. S1E.

Scale bars: 20 μm.

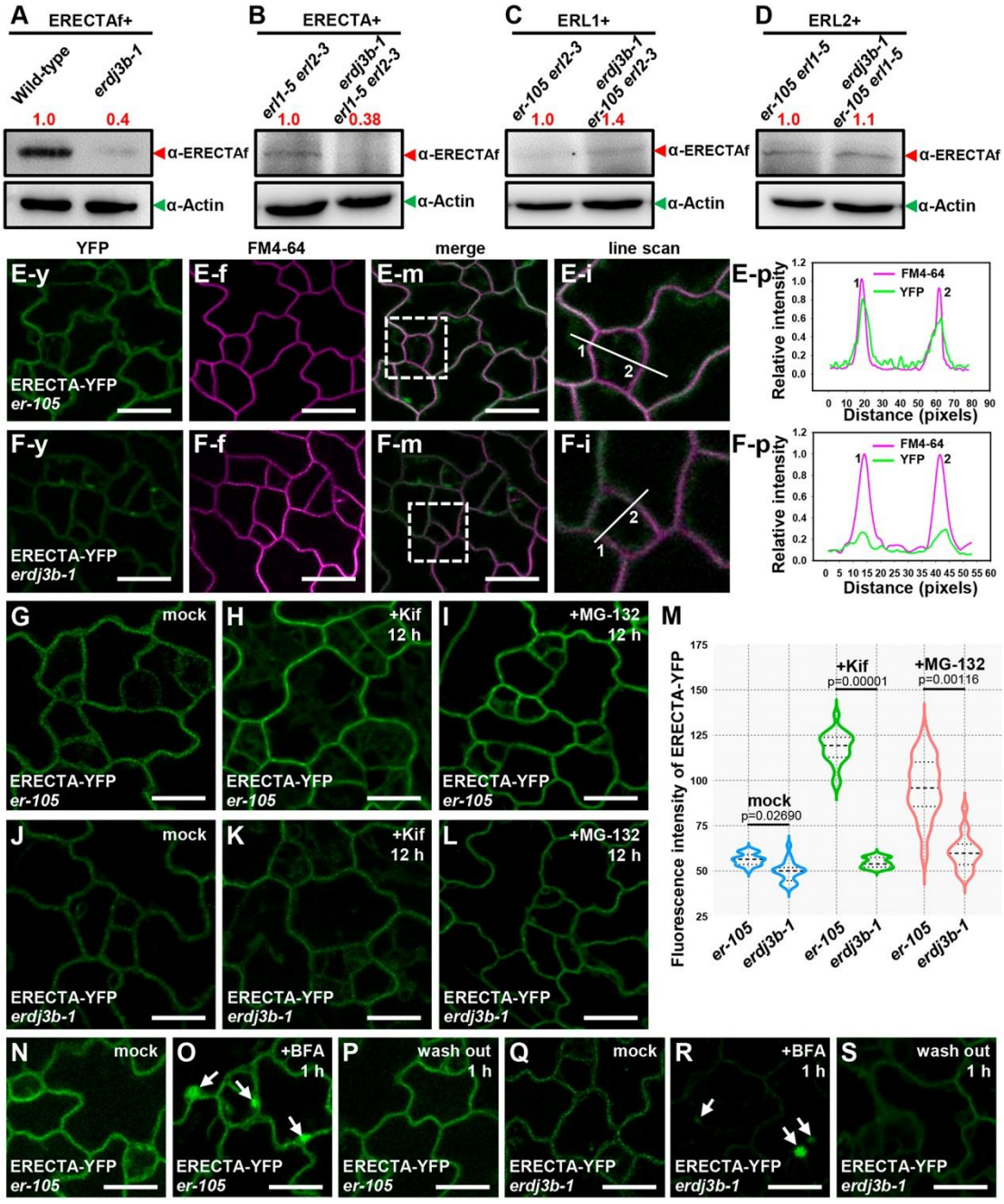

Fig. 2. Mutation of *erdj3b* affects the protein abundance but not the localization of ERECTA.

(A-D) Immunoblot analysis of protein amount using antibodies that recognize all ERECTA-family proteins (red arrowhead). The numbers above the upper panel are relative ratios of mean gray values of bands to wild-type. Lower panel, the loading control detected with anti-Actin (green arrowhead). (E) Colocalization analysis of ERECTA-YFP (*er-105* complementary) and FM4-64

dye. ERECTA-YFP and FM4-64 fluorescence intensity profiles are quantified along a transect crossing stomatal precursor cells (line scan, indicated by a white line). (F) In *erdj3b-1*, ERECTA-YFP fluorescence intensity is greatly reduced at the PM, comparing with FM4-64. (G-L) Expression level of ERECTA-YFP is enhanced after 12 h treatment with 20 μM Kifunensine (Kif) or 40 μM MG-132, but not in *erdj3b-1* mutant background. (M) Quantification of fluorescence intensity in stomatal precursor cells. The Kif- and MG-132-induced enhancement of ERECTA-YFP is significantly suppressed in *erdj3b* mutant. Student's *t*-test was performed between *er-105* and *erdj3b-1* (n=21). (N-S) Application of 50 μM BFA induces aggregation of ERECTA-YFP in BFA-bodies (white arrows), an effect that is reversed after wash-out. ERECTA-YFP in *erdj3b-1* displays a similar response to BFA.

Scale bars: 20 μm.

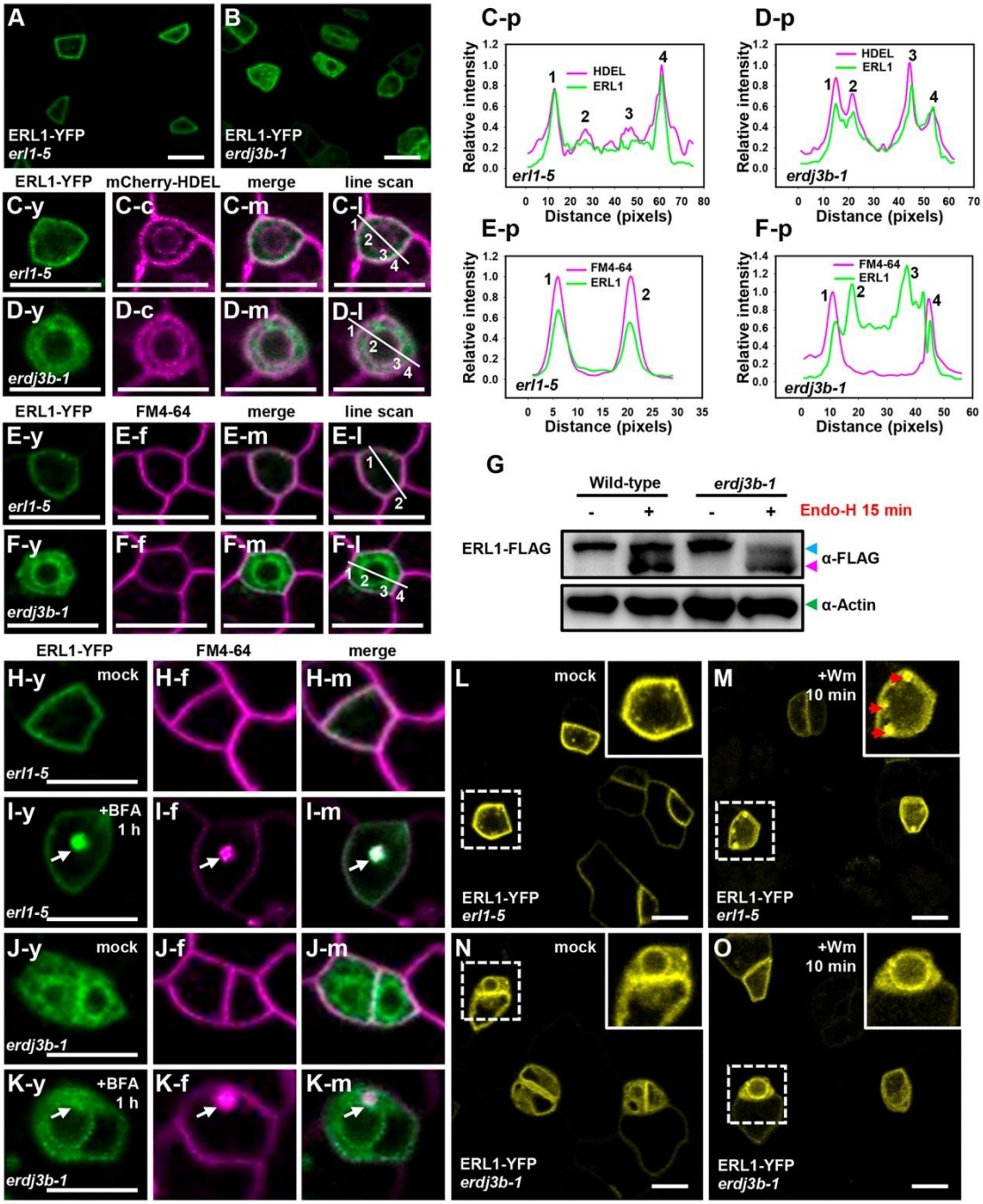

Fig. 3. Mutation of *erdj3b* mainly affects the subcellular localization of ERL1.

(A, B) ERL1-YFP (*erl1-5* complementary) predominantly localizes at the PM of stomatal lineage cells. In *erdj3b-1*, ERL1-YFP is found in ring-like structure surrounding the nucleus. (C, D) Colocalization ERL1-YFP with ER marker mCherry-HDEL in *erdj3b-1* stomatal precursor cells is confirmed by quantitative analysis of fluorescence intensity profiles. (E, F) Colocalization of

ERL1-YFP with FM4-64 dye at the PM is reduced in *erdj3b-1*. Line scan profiles demonstrates the change of ERL1-YFP localization from the PM to the ER. (G) Immunoblot analysis of ERL1-FLAG protein in Endo-H assay. ERL1-FLAG extracted from *erdj3b-1* plants is sensitive to Endo-H, showing a stronger lower band (cleaved proteins, pink arrowhead). (H-K) After 1 h treatment with 50 μM BFA, ERL1-YFP colocalizes with FM4-64 in BFA-bodies (white arrow). However, ERL1-YFP in *erdj3b-1* fails to colocalize with FM4-64 in BFA-bodies. (L-O) Application of 25 μM Wortmannin (Wm, 10 min) induces the formation YFP-positive Wm-bodies (red arrows in inset) but not in *erdj3b-1* mutant precursor cells.

Scale bars: 20 μm.

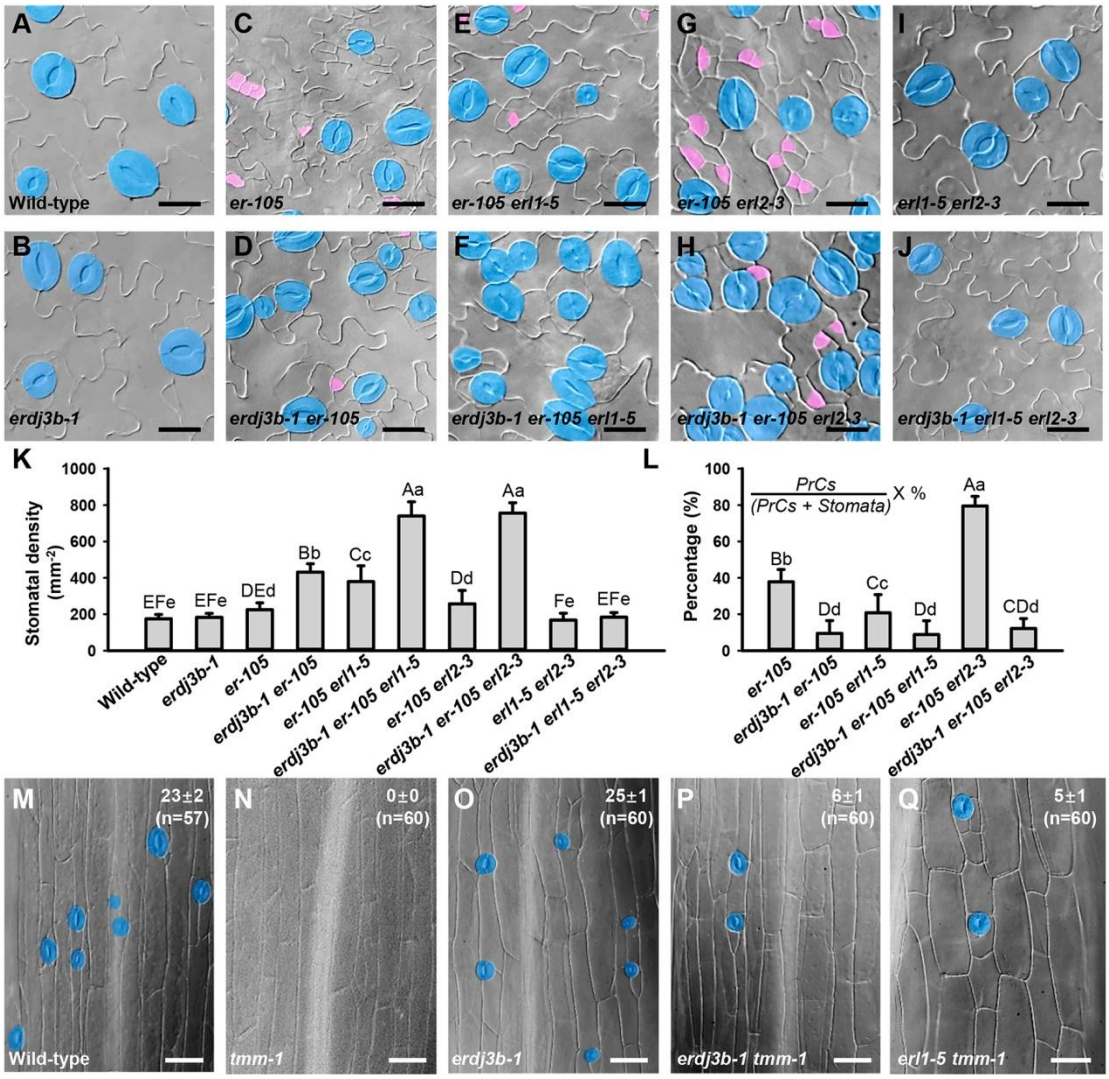

Fig. 4. ERECTA-family receptors are distinctly regulated by the ERQC system.

(A-J) DIC images of 12-day-old cotyledons. Mature stomata and Precursor-like Cells (PrCs) are highlighted by blue and pink color, respectively. Mutation of *erdj3b* promotes the differentiation of PrCs into mature stomata and stomatal clusters in *er-105*, *er-105 erl1-5*, and *er-105 erl2-3*. (K, L) Quantitative analysis of stomatal density and percentage of PrCs over the total number of PrCs and stomata. Values are mean ± s.d (n=18). Data were analyzed using ANOVA. The different uppercase and lowercase letters indicate significant differences at 1% and 5% levels, respectively. (M-Q) Mutation of *erdj3b*, like *erl1*, can restore the stomatal formation of hypocotyls

in the *tmm-1*. The numbers at upper right corner are the number of stomata per hypocotyl (mean ± s.d).

Scale bars: 20 μm.

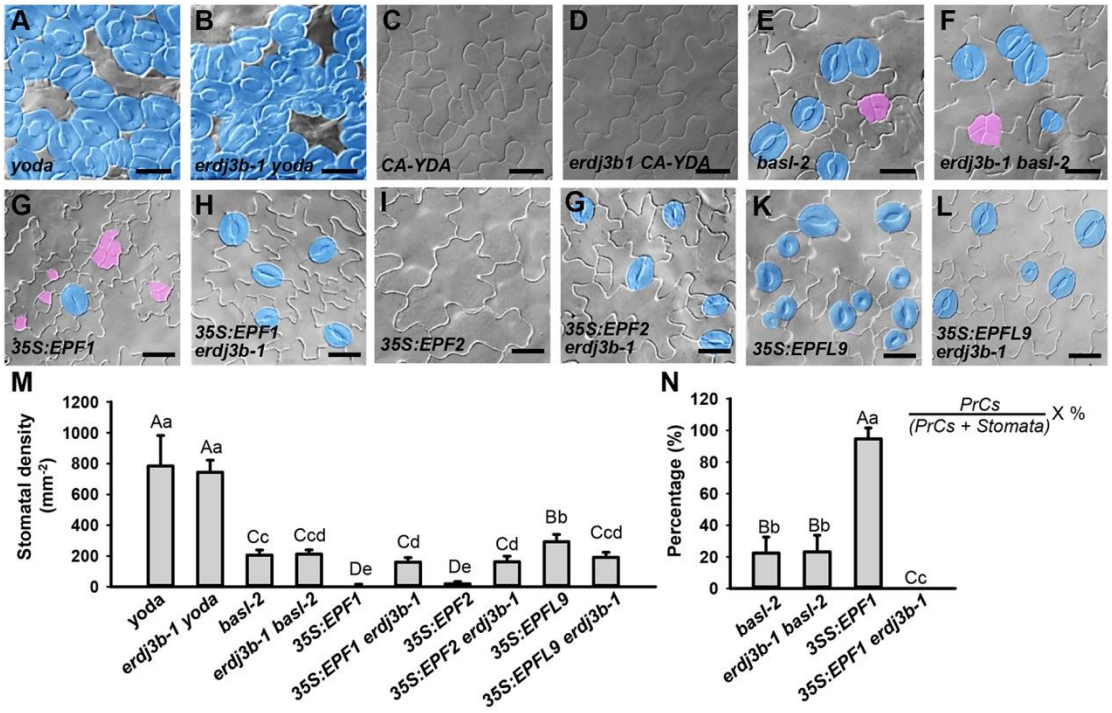

Fig. 5. Function of ERdj3B is required for signaling transduction of peptide ligands upstream of YODA.

(A, B) Mutation of *erdj3b* has no impact on the stomatal phenotype in *yoda.* Large stomatal clusters were found in both *yoda* (A) and in *erdj3b-1 yoda* (B). (C, D) No stoma was found in the *CA-YDA* (C) and *erdj3b-1 CA-YDA* (D). (E, F) Mutation of *erdj3b* has no impact on the stomatal phenotype of *basl-2.* Similar stomatal clusters and small-cell clusters (highlighted by pink color) are found in both *basl-2* (E) and *erdj3b-1 basl-2.* (G-H) Overexpressing of *EPF1* promotes over-proliferative divisions in epidermal cells (highlighted by pink color) (G), but, the effect of *EPF1* overexpression is abolished in a *35S:EPF1 erdj3b-1* transgenic line (H). (I-J) Overexpressing *EPF2* inhibits stomatal production in a *35S:EPF2* transgenic (I), but stomatal production can be resumed in *35S:EPF2 erdj3b-1* transgenic (J). (K, L) Overexpression of *EPFL9* promotes stomatal production is a *35S:EPFL9* transgenic line (K), the stomatal production is normal in a *35S:EPFL9 erdj3b-1* transgenic line (L). (M, N) Quantitative analysis of stomatal density (M) and percentage of PrCs (N) over the total number of PrCs and stomata. Values are mean ± s.d (n=18).

Data were analyzed using ANOVA. The different uppercase and lowercase letters indicate significant differences at 1% and 5% levels, respectively.

Scale bars: 20 μm.

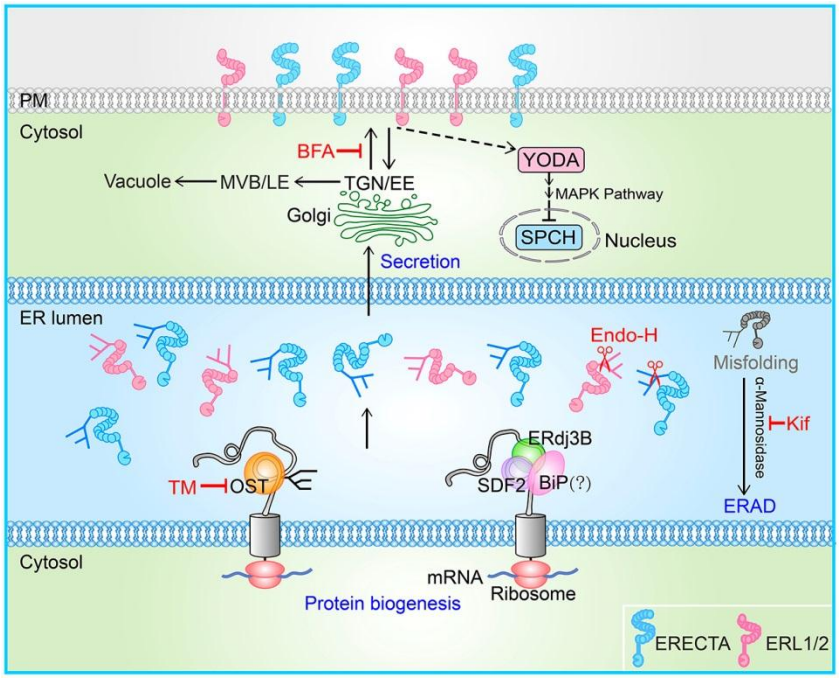

Fig. 6. Model of SDF2-ERdj3B-BiP chaperon complex regulating stomatal development.

Schematic model of regulation of ERECTA-family receptors by ERQC. Inhibition of N-glycosylation by TM significantly affects ERECTA-family receptors protein abundance and subcellular localization. Endo-H enzyme primarily cleaves off N-linked glycans of ER-localized proteins. Function of SDF2-ERdj3B-BiP chaperon complex is required for ERECTA-family protein biogenesis in the ER lumen and transport from the ER to the plasma membrane, where lastly activate the downstream YODA-MAPK cascade for regulating stomatal development. Improperly or incompletely folded proteins are retained in the ER for further folding or ultimately degraded by ERAD. Kifunensine, an inhibitor of ER mannosidase, prevents misfolded protein to degrade via the ERAD pathway.

Fig. S1

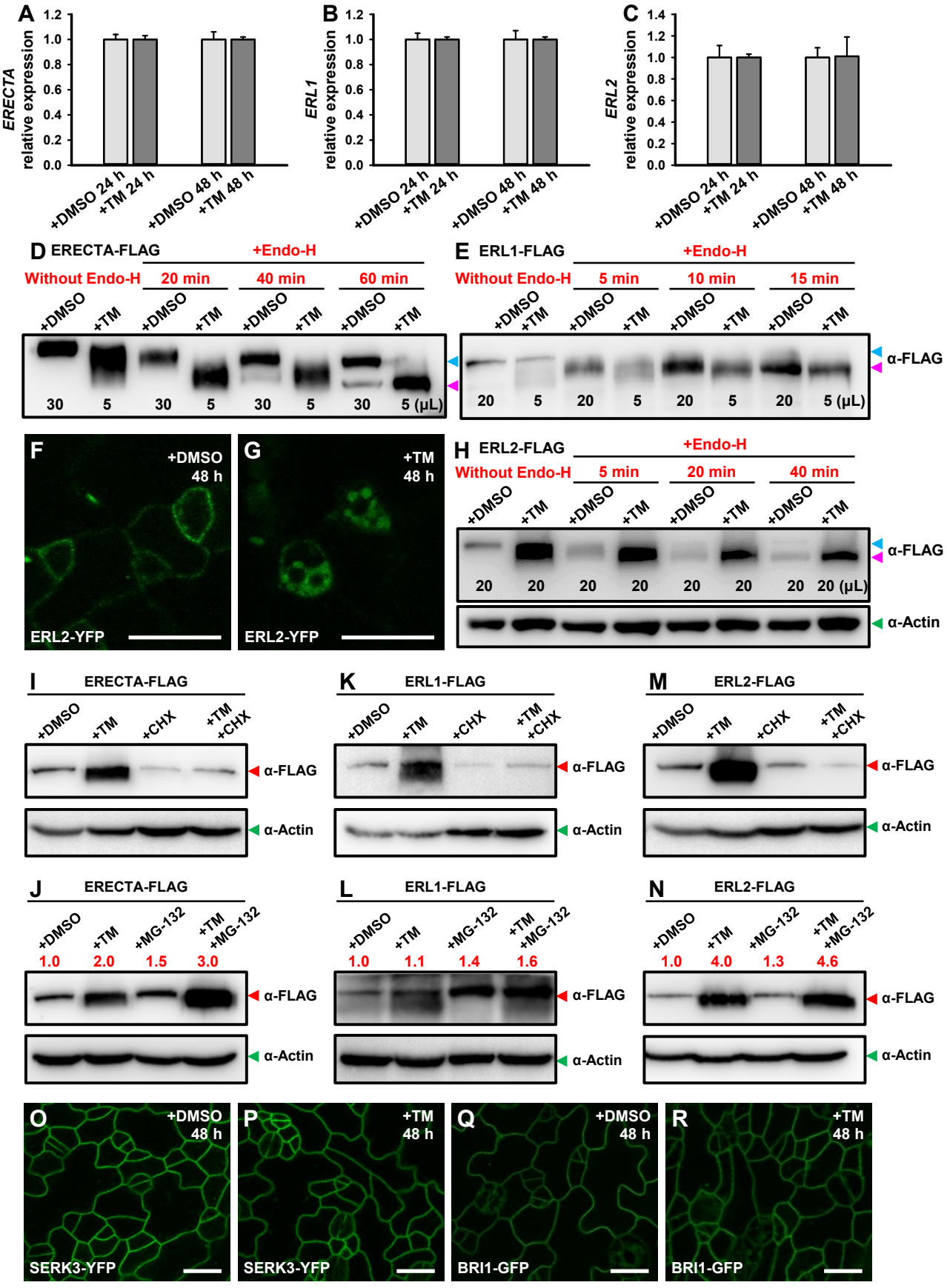

Fig. S1. Endo-H assay of ERECTA-family proteins and ERL2-YFP expression after TM treatment.

(A-C) RT-qPCR analysis of the transcription levels of ERECTA-family genes. No significant differences are found between DMSO and TM treatments. Data are mean ± SD of three biological replicates. (D) Immunoblot analysis of ERECTA-FLAG protein extracted from mock (DMSO) and TM-treated plants with and without Endo-H digestion. ERECTA-FLAG protein from TM-treated plants are sensitive to Endo-H digestion, showing a stronger lower band (cleaved proteins) in immunoblot after Endo-H digestion (pink arrowhead). Prolonged Endo-H digestion of 40 min or 60 min produces two bands in control plants. While, the upper band (non-cleaved proteins) is not detected in TM-treated plants (blue arrowhead). The samples without Endo-H digestion are presented as control (left two lanes). Notice the fast moving of ERECTA-FLAG protein from the TM-treated plants. (E) Immunoblot analysis of ERL1-FLAG protein after Endo-H digestion. ERL1-FLAG protein from TM-treated plants are sensitive to Endo-H digestion, showing a faster mobility in immunoblot. (F, G) Confocal images of *ERL2:ERL2-YFP* in epidermis. Strong ERL2-YFP signals are detected inside the stomatal precursor cells after TM treatment. (H) Immunoblot analysis of ERL2-FLAG protein with and without Endo-H digestion. In contrast to the two bands of ERL2-FLAG in control plants (blue and pink arrowheads), Endo-H digestion of ERL2-FLAG protein from TM-treated plants results in a single band with faster mobility. Lower panel, the loading control of actin detected by anti-Actin (green arrowhead). (I-N) Immunoblot analysis of ERECTA-FLAG, ERL1-FLAG and ERL2-FLAG protein extracted from mock (DMSO), and treated with TM, CHX, TM with CHX, MG-132, and TM with MG-132. Top panel, the ERECTA family protein bands detected by anti-FLAG (red arrowhead). Lower panel, the loading control of actin detected by anti-Actin (green arrowhead). The red numbers above the upper panel are relative ratios of mean gray values of bands to the DMSO control. (O-R) No obvious changes of SERK3-YFP and BRI1-GFP in epidermis after TM treatment. Scale bars: 20 μm.

Fig. S2

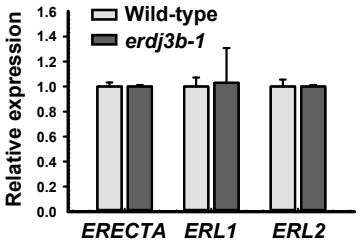

Fig. S2. RT-qPCR analysis of the transcription levels of ERECTA-family genes. No significant differences are found between wild-type and *erdj3b-1* mutant. Data are mean ± SD of three biological replicates.

Fig. S3

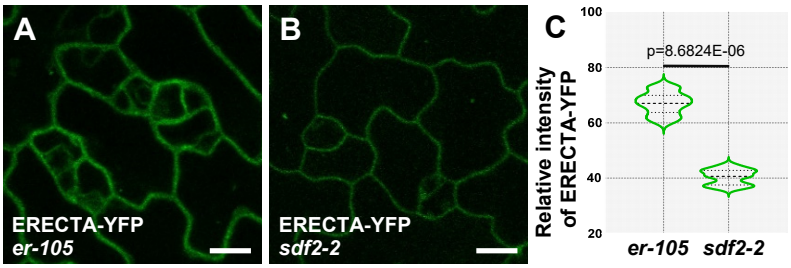

Fig. S3. The overall fluorescence intensity of ERECTA-YFP is reduced in *sdf2-2* mutant.

(A, B) Confocal images of ERECTA-YFP in *er-105* (complementary) and *sdf2-2* mutant leaf epidermis. Scale bars: 20 μm. (C) Quantification fluorescence intensity in stomatal precursor cells. ERECTA-YFP intensity in *er-105* is statistically different from that in *sdf2- 2* after student's *t*-test (n=21). The middle value of each violin plot is displayed as a dotted line.

Fig. S4

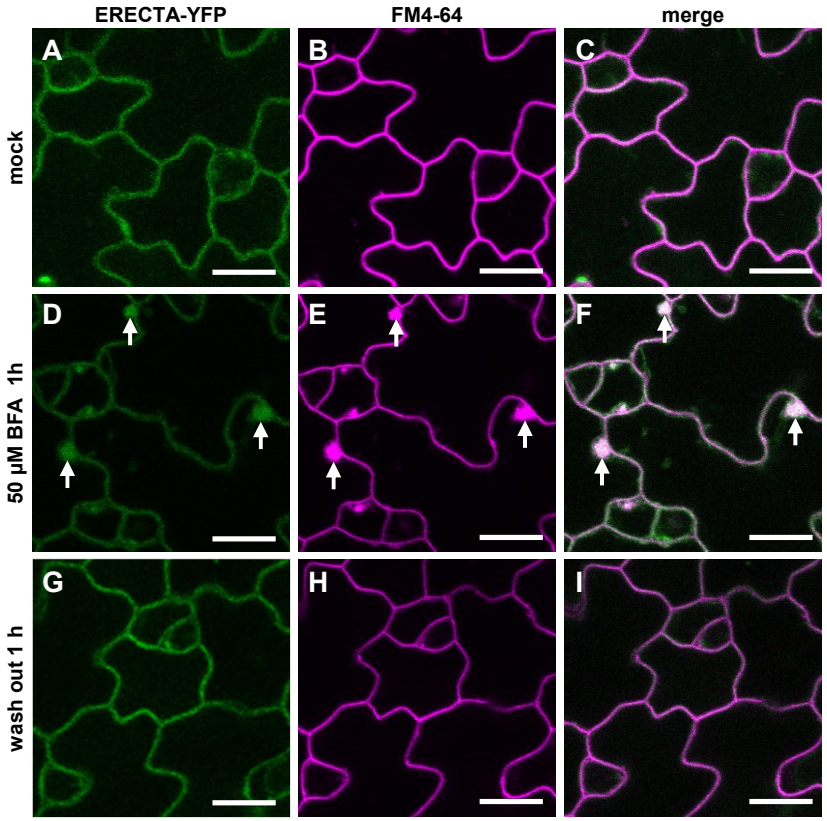

Fig. S4. Effects of BFA on subcellular localization of ERECTA-YFP.
(A-C) Confocal images show the colocalization of ERECTA-YFP (*er-105* complementary) with FM4-64 at the PM. (D-F) Confocal images show the aggregation of ERECTA-YFP and FM4- 64 in BFA-bodies (white arrows) at 1h after 50 µM BFA treatment. (G-I) Confocal images show the colocalization of ERECTA-YFP colocalizes with FM4-64 at the PM in BFA-treated plants after 1 h water rinse (wash out).
Scale bars: 20 µm.

Fig. S5

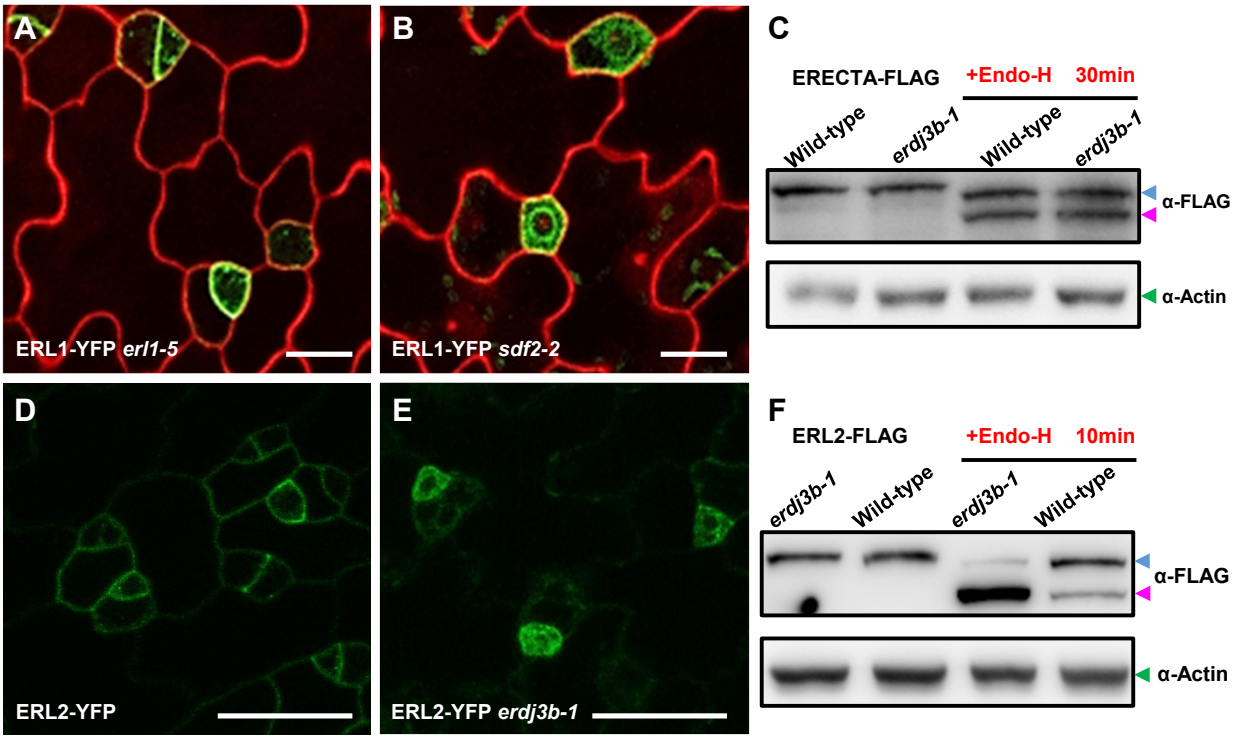

Fig. S5. Dysfunction of SDF2-ERdj3B-BiP complex causes retention of ERL1 and ERL2 in the ER.

(A, B) ERL1-YFP (*erl1-5* complementary) predominantly localizes at the PM in stomatal precursor cells. In *sdf2-2*, ERL1-YFP is present in ring-like structure. Cell outlines are visualized with propidium iodide. (C) Immunoblot analysis of ERECTA-FLAG after Endo-H digestion. ERECTA-FLAG proteins extracted from wild-type and *erdj3b-1* plants show a similar response to Endo-H digestion. A blue and a pink arrowhead indicate the non-cleaved proteins (upper band) and cleaved proteins (lower band), respectively. Lower panel, loading control of actin detected by anti-Actin. (D, E) ERL2-YFP predominantly resides at the PM of stomatal precursor cells in the wild-type plants. In *erdj3b-1,* strong ERL2-YFP signals are detected in the ring-like structure. (F) Immunoblot analysis of ERL2 after Endo-H digestion. ERL2-FLAG protein extracted from *erdj3b-1* plants are sensitive to Endo-H digestion, comparing with ERL2-FLAG in wild-type plants, showing a stronger lower band (cleaved proteins) in immunoblot analysis. Scale bars: 20 μm.

Fig. S6

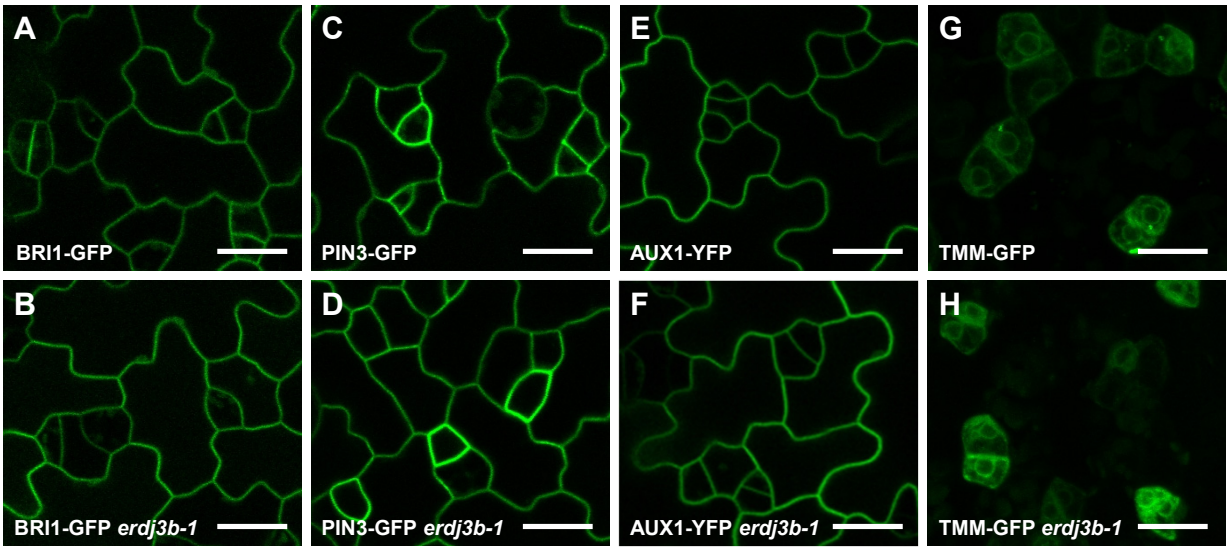

Fig. S6. BRI1-GFP, PIN3-GFP, AUX1-YFP and TMM-GFP expression in wild-type and *erdj3b-1* epidermis.

(A-H) No obvious changes of BRI1-GFP, PIN3-GFP, AUX1-YFP, and TMM-GFP expression and localization are found in *erdj3b-1* mutant epidermis, comparing in wild-type background. Scale bars: 20 μm.

Fig. S7

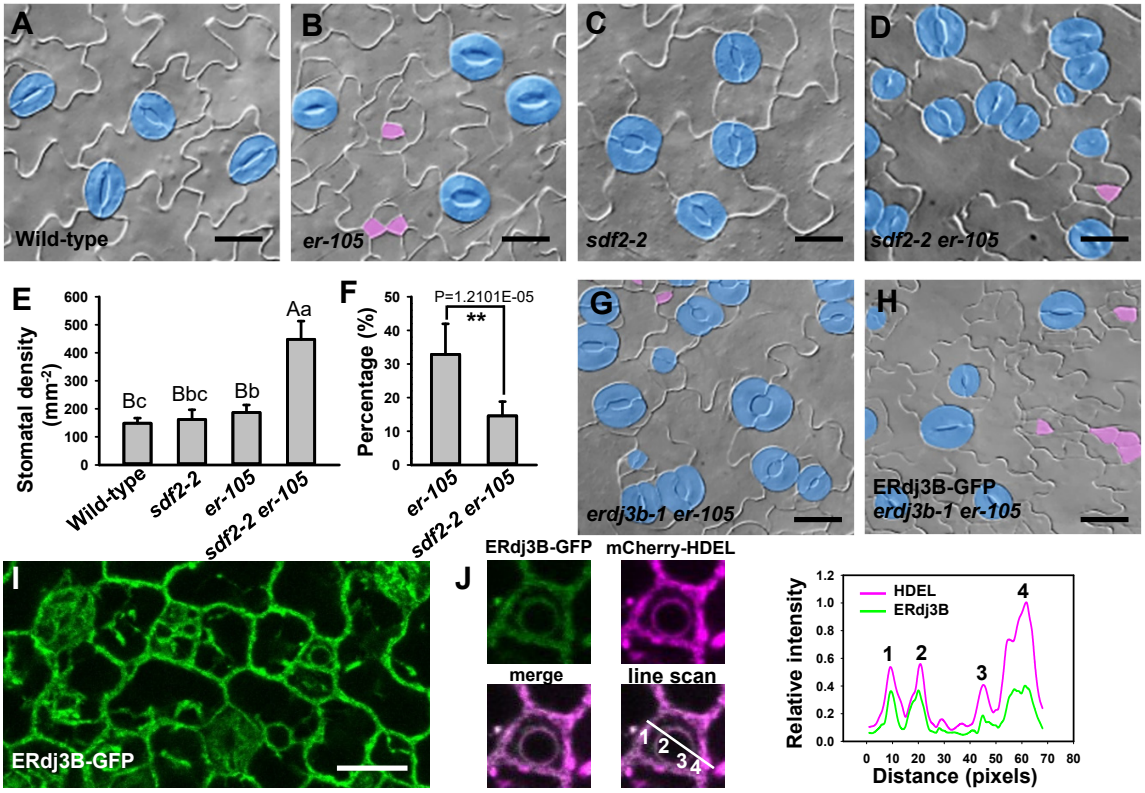

Fig. S7. ER-resident SDF2-ERdj3B-BiP is differentially involved in stomatal development regulation.

(A-D) DIC images of 12-day-old cotyledons. Mature stomata are highlighted by blue color. Precursor-like Cells (PrCs) are highlighted by pink color. Mutation of *sdf2* promotes the differentiation of PrCs in *er-105* into mature stomata, leading to an increase of stomatal production and stomatal clusters. (E) Quantitative analysis of stomatal density. Values are mean± SD (n=18). The different uppercase and lowercase letters indicate significant differences at 1%and 5% levels, respectively, after ANOVA analysis. (F) Quantification of the percentage of PrCs over total number of PrCs and mature stomata. Values are mean ± SD. Asterisks indicate significant difference after Student's two-tailed *t*-test, ***P*<0.01. (G, H) Introduction of *ERdj3B:ERdj3B-GFP* restores the appearance of arrested precursor cells in *erdj3b-1 er-105*, resembling the stomatal phenotype in *er-105* single mutant. (I, J) Confocal image of *ERdj3B:ERdj3B-GFP* expression in epidermis cells. ERdj3B-GFP is colocalized with the ER marker mCherry-HDEL in a stomatal precursor cell. Quantitative analysis of fluorescence intensity profiles (line scan) reveals the colocalization of ERdj3B-GFP with mCherry-HDEL in the ER. Scale bars: 20 μm.

Table S1.

Click here to download Table S1